Development and Validation of a Human-Body Mathematical Model for Simulation of Car-Pedestrian Collisions

J. K. Yang and P. Lövsund

Dept. of Injury Prevention, Chalmers University of Technology, Sweden

ABSTRACT

The aim of this study was to develop a 3D mathematical model of the human body to simulate responses of pedestrians in car impacts with emphasis on the lower extremities and the head. The model, implemented by using MADYMO-GEBOD program, consists of fifteen body segments connected by fourteen joints, including two human-like knee joints and two breakable leg segments which allow to simulate the knee responses associated with leg fracture.

The model was verified by using published sled impact tests with cadavers in terms of kinematics of the pedestrian substitutes, accelerations of the body segments, and failure description from anatomical investigations of the pedestrian substitutes. The sensitivity of the model to input variables was studied at impact speeds of 15 and 40 km/h with the following parameters: bumper height, bumper stiffness, bumper lead distance, height of hood-edge, hood-edge stiffness, and impact speed. The validated model demonstrated its capability in simulations of car-pedestrian impacts to predict risk of pedestrian injuries and to develop safety countermeasures for pedestrian protection.

DURING THE PAST TWO DECADES, even though significant reductions in pedestrian fatalities have been achieved in the European Union and in the United States, there is still a high proportion of pedestrian fatalities in all killed road users over the world. The relative frequency of pedestrian fatalities vary from 13.5% in the USA (NHTSA, 1995), 18.8% in the EU (ETSC, 1993) to 47% in Thailand (Mohan *et al*., 1995). Pedestrian protection is therefore a priority item in traffic safety strategies (EEVC, 1985; ETSC, 1997). There is a need for developing effective safety countermeasures based on a better knowledge of the pedestrian responses and injury mechanisms in accidents as well as on an effective approach to predict risk of pedestrian injuries.

For more than 30 years, pedestrians impacted by vehicles have been the concern of many studies carried out in the field of traffic safety. The impact responses and injury mechanisms of the body segments in this type of accidents have been widely investigated with cadavers (Pritz, 1978; Cavallero *et al*., 1983; Bunketorp *et al*., 1983; Aldman *et al*., 1985) and pedestrian dummies (Cesari *et al*, 1982; Brun-Cassan *et al*., 1983; Glaeser, 1983; Schlumpf and Niederer, 1987). The best understanding of responses and injury mechanisms of body segments in car-pedestrian collisions has been achieved from tests with cadavers. Cadaver tests, however, can not be used for extensive study of safety countermeasures due to limitation of available subjects and high costs for such tests. Several types of dummies were developed in order to evaluate new safety countermeasures, so far none of them was representative enough to simulate responses of pedestrians in car impacts (Niederer *et al*., 1983; EEVC, 1985). Earlier studies (Padgaonkar *et al*., 1977; Appel *et al*., 1978; Ashton, 1978) indicated that the problem of pedestrian protection from a car impact involves a large number of variables, such as the impact speed in accident, the type and size of the car, geometry and stiffness of the car front, as well as the size and age of the pedestrian. Obviously, it is impractical to perform experimental studies of the effect of all variables on car-pedestrian impacts.

A simple mathematical model of pedestrian was first used by Padgaonkar *et al*. (1977) to simulate vehicle-pedestrian impacts. Since the beginning of the 80's, pedestrian mathematical models are available in the MADYMO (Wismans and van Wijk, 1982; Janssen and Wismans, 1986). In one 15-

segment pedestrian MADYMO model developed by van Wijk *et al.* (1983), the input data set (e.g. the geometry, mass, moment of inertia and joint characteristics) was derived from the mechanical Hybrid II dummy. Analysis of the results from previous computer simulations of pedestrian impacts shows that the early pedestrian models are not fully comparable with the experiments performed with biological subjects. The deficiencies are the limited lateral flexibility and the undeformable elements in the model. Furthermore the impact responses of the knee cannot be properly simulated. Thus, it was found desirable to develop a mathematical model based on available biomechanical data from human subject experiments. Such a model should be able to describe responses of the human body in vehicle-pedestrian accidents as close to reality as possible.

Gibson *et al.* (1986) developed a pedestrian 2D mathematical model to investigate head impact response in car-pedestrian crashes. However, the 2D model was not suitable to simulate dynamic responses of pedestrians in crash environment. A complicated spatial motion of the impacted pedestrians may result from: (1) different initial postures of the pedestrians; (2) successive impacts to the body segments in a large relative movement between pedestrian and moving car; (3) 3D distribution of the center of gravity of body segments. Some of the injury parameters related 3D motion can not be analysed by a 2D mathematical model (Schlumpf and Niederer, 1987). Ishikawa *et al.* (1993) developed a pedestrian 3D mathematical model to analyze the influence of car front parameters on pedestrian injuries. Biomechanical data of human body were used to describe this model which shows more realistic response in modeling car-pedestrian collisions than pedestrian mathematical models based on dummy data. The deficiency of the 3D model was lack of sufficient description for knee joints and leg segments, so that it can not simulate responses of the knee and leg in details.

A 3D human-like knee joint model (Yang and Kajzer, 1993) was developed as a first step towards a whole human-body model. The aim was to achieve a good correlation with knee responses in tests with human specimens. The human-like knee model is based on the anatomic structure of the knee and implemented in a one-legged pedestrian model. Furthermore, a 3D breakable leg model (Yang *et al.*, 1993; Yang, 1997) was developed to improve biofidelity of the pedestrian model in simulation of a car-pedestrian impact with leg fracture. The breakable leg model consists of two elements connected by a frangible joint, which is able to simulate leg fracture in lateral impacts.

Furthermore there is a need for a mathematical model of the whole human body with good biofidelity. Such a model should be able to accurately describe responses of the human body in vehicle-pedestrian accidents. The present paper describes the development and validation of a human-body 3D mathematical model with the human-like knee model and the breakable leg model. The human-body model is to be used as a pedestrian substitute to study car-pedestrian impact interactions and to predict risk of pedestrian injuries in accidents.

METHOD

The MADYMO-GEBOD package (TNO, 1996) was used to develop a human-body 3D mathematical model for the study of kinematics and biomechanics of pedestrians involved in car crashes. The GEBOD (Baughman, 1983) provides the anthropomorphic data of the human body for adults and children of various sizes, based on a set of thirty-five measurements of body dimensions. A 3D stereophotometric adult body database from sample populations is available in the GEBOD and used to calculate regression equations for specific body data set as function of body height and/or body weight. The data set for a human-body model includes the geometry, mass distribution, location of center of gravity, and moment of inertia of all body segments as well as location of the joints. The MADYMO provides a solver to analyze the dynamic responses of systems undergoing gross motion, by modeling such structures as multiple bodies connected by joints.

The human-body model was used as a pedestrian substitute in simulations of car-pedestrian impacts. Validity of the model was evaluated against published crash tests with cadavers and a car-front which mounted on a sled (Ishikawa *et al.*, 1993). The sensitivity of the model to input variables was studied by varying parameters of car-front in simulations of car-pedestrian impacts.

THE HUMAN-BODY MODEL - Figure 1 shows the configuration of the human-body model in standing position, which is generated by the GEBOD program based on the 50th percentile male adult (height 175 cm, total body mass 78 kg). The model consists of fifteen ellipsoids representing the following body segments: head, neck, thorax, abdomen, pelvis, left/right arm, left/right forearm, left/right thigh, left/right leg, and left/right foot. The body segments are connected to each other by 14

joints. The knee joints and the leg elements generated by the GEBOD have been replaced with a human-like knee model (Yang and Kajzer, 1993) and a breakable leg model (Yang, 1997) as shown in Figure 4.

Mass distribution and moment of inertia - The mass of the body segments, the location of joints, and the principal moments of inertia of the body segments were derived by the GEBOD program based on the regression equations from the stereophotometric data.

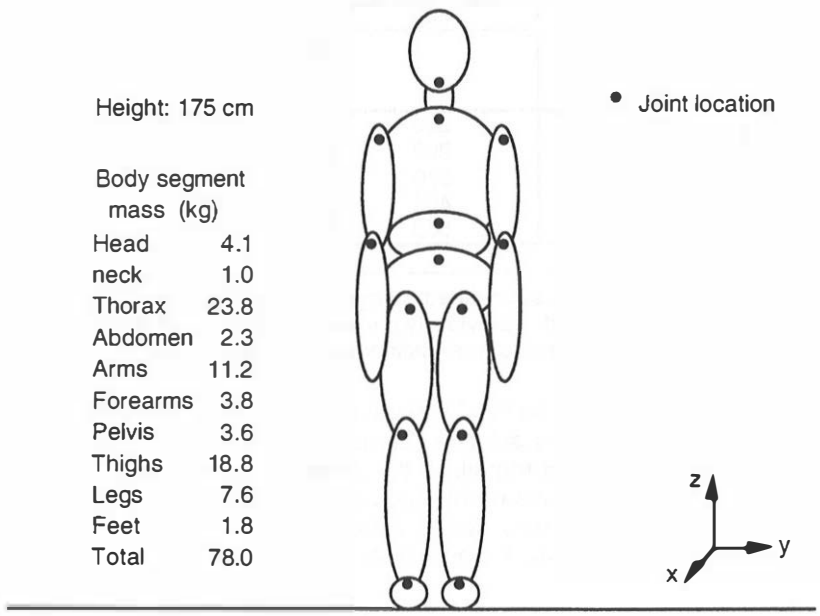

Figure 1. Human body model of a 50th percentile adult male: geometry (the hand is combined with forearm), mass distribution, and joint location.

Stiffness of the body segments - The major experimental studies on strength and tolerance of the human body segments to lateral impact loading are summarized in Table 1. These studies provide the information for characterization of the body segments in the mathematical model. In the MADYMO, mechanical properties of body segments are described by a force-deformation function.

Table 1
Summary of main studies on strength and tolerance of the human body segments

Segment	Peak force to failure	Deformation	Authors
Head	5.2 - 12.5 kN	3 - 3.5 mm	Voigt *et al.*, 1973; Stalnaker *et al.*, 1977; Allsop *et al.*, 1991.
Thorax	5.5 - 10.2 kN	35 - 38.4% *	Tarrierre *et al.*, 1979; Viano, 1989.
Abdomen	6.73 kN (mean)	43.7% *	Viano *et al.*, 1989.
Pelvis	9 - 12.5 kN	~ 40 mm	Cesari *et al.*, 1983; Viano *et al.*, 1989.
Arm	2.71 - 4.16 kN	~ 9 mm	Messerer, 1880; Yamada, 1970; Cesari *et al.*, 1981.
Forearm	2.4 kN (mean)	~ 10 mm	Messerer, 1880; Yamada, 1970;
Thigh	2 - 10 kN	~ 11 mm	Yamada, 1970; Kress *et al.*, 1993.
Leg	2 - 8 kN	~ 8 mm	Bunketorp *et al.*, 1983; Nyquist *et al.*, 1985; Kress *et al.*, 1993

* Lateral compression to the thorax and the abdomen.

Table 2 shows the stiffness defined in the model for different body segments. The stiffness of the body segments were derived with average values from these studies (Table 1) and used to describe mechanical properties of the body segments in the model in the form of a force-deformation function. In the initial phase of the force-deformation function defined for the body segments a low stiffness was used, taking into account the effect of soft tissues covering the bones on the contact characteristics between body segment and car component. The soft tissue stiffness used in the model is based on mechanical properties of skin and muscle reported by Yamada (1970). The contact stiffness for the

body segments changes from soft tissue stiffness to bone stiffness at 3 mm deflection for the head, 30 mm for the pelvis, 25 mm for the arms, 40 mm for the thighs, and 30 mm for the legs.

Table 2
The stiffness of body segments defined in the present study

Body segment	Bone stiffness (N/mm)	Stiffness of soft tissues (N/mm)
Head	2500	150
Neck	rigid*	
Thorax	100**	
Abdomen	80**	
Pelvis	330	35
Arm	300	20
Forearm	270	25
Thigh	400	25
Leg	500	30
Foot	rigid*	

* Neck and foot segments were defined as rigid elements due to the fact that no direct impact was observed in previously performed experiments with cadavers.
** Thorax and abdomen segments were defined with overall stiffness.

Joint models - From an anatomical point of view, the human-body joints are very complex. In a multibody model, the human-body joints are represented by mechanical joint models such as the spherical joint model and the hinge joint model. In the present study, the spherical joint model was used to describe biomechanical responses of the neck joint, torso joint, hip joint, shoulder joint, and ankle joint, and the hinge joint model was used to describe the elbow joint. The knee joint was described by a human-like knee joint model (Yang, 1997).

Motion of joints - In order to characterize the joint models, the motion range of joints are summarized in Table 3 based on the main studies by Kapandji (1970a,b,c), White and Panjabi (1978), and Frankel and Nordin (1980). In general, the physiology movements of joints are defined in a coordinate system formed by three planes: the sagittal, coronal, and horizontal planes. The flexion-extension movements of joints are performed in the sagittal plane, and the abduction-adduction movement in the coronal plane. The rotation movements of joints are performed about longitudinal axis of body segment. The motion of the cervical-vertebral column has been taken into account for the definition of the neck joints, and the motion of the thoracic and lumbar vertebral column has been taken into account for definition of the torso joints.

Table 3
The joint motion range used to define joint models
(based on Kapandji, 1970a,b,c ; White and Panjabi, 1978; Frankel and Nordin, 1980)

Physiological feature	Motion range of joints (degree)							
	Upper-neck	Lower-Neck	Upper-torso	Lower-torso	Shoulder	Elbow	Hip	*Ankle-subtalar
Flexion	10	30	45	60	180	145 - 160	90 - 145	20 - 30
Extension	15	60	25	35	45 - 50	0	20 - 30	30 - 50
Abduction					140	0	45	30 - 40
Adduction					30 - 45	0	30	25 - 35
Lateral rotation					80	90	30	
Medial rotation					95	85	60	
Inversion								15 - 20
Eversion								10 - 15
Lateral flexion	±10	±35	±20	±20				
Axial rotation	±10	±40	±35	±5				

* The motion of the ankle is combined with that of the subtalar joint.

Stiffness of joints - Based on biomechanical studies on human joints (Table 4), the joint stiffness within the range of normal joint motion was chosen to describe the characteristics of joint models used in the present study. Figure 2 shows the moment-angle functions of the joint models according to the data summarized in Tables 3 and 4 .

Table 4
The characteristics of the joints
(based on Kapandji, 1970a,b,c; Mertz & Patrick, 1971; Nyquist & Murton, 1975; Frankel & Nordin, 1980; Wismans & Spenny, 1983; Wismans *et al.*, 1986; McElhaney *et al.*, 1988; Osvalder, 1992; Parenteau & Viano, 1996)

Physiological feature	Stiffness (Nm/degree)							
	Upper-neck	Lower-Neck	Upper-torso	Lower-torso	Shoulder	Elbow	Hip	Ankle-subtalar
Flexion	1.4	1.4	1.0 - 2.1	1.0 - 2.1	0 - 0.3	0 - 0.2	0 - 2.5	0.5
Extension	2.5	2.5	0.3 - 1.8	0.3 - 1.8	0 - 0.2		1.2	0.3
Abduction					0 - 0.3		0 - 1.2	-
Adduction					-		0.8	-
Lateral rotation					0.3	0.2	0.6	
Medial rotation					0.3	0.2	0.6	
Inversion								1
Eversion								1.5
Lateral flexion	0.4 - 2.2	0.4 - 2.2	2.0	2.0				
Axial rotation	0.0 - 0.5	0.0 - 0.5	0.9	0.9				

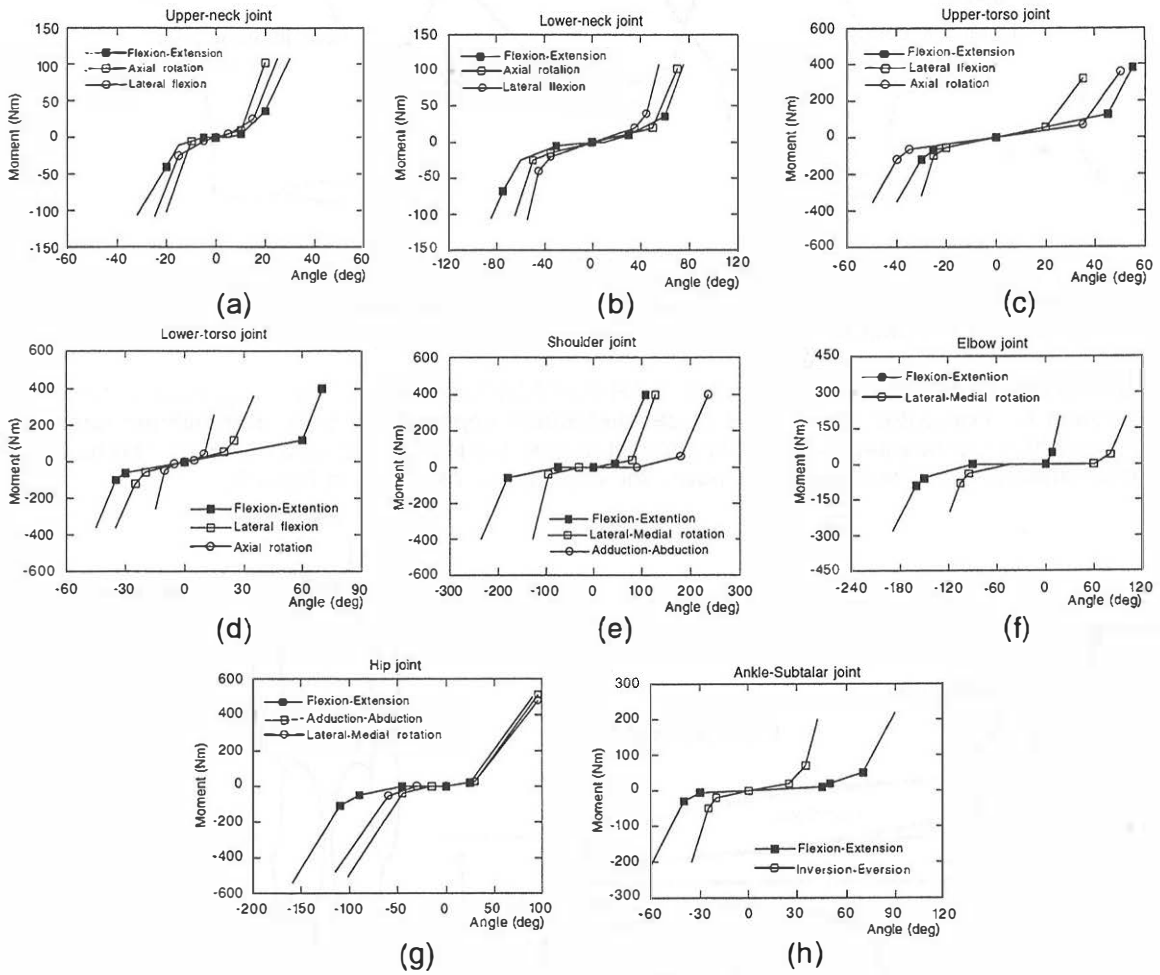

Figure 2. Moment-angle characteristics of the joints in the human-body mathematical model: (a) upper-neck joint, (b) lower-neck joint, (c) upper-torso joint, (d) lower-torso joint, (e) shoulder joint, (f) elbow joint, (g) hip joint, and (h) ankle-subtalar joint.

Human-like knee joint model - Figure 3 shows the configuration of the knee joint model. A detailed description of the human-like knee model was given by Yang *et al.* (1995).

Breakable leg model - The basic configuration of the breakable leg model was two rigid elements connected by a spherical joint. The spherical joint between these two elements located at the bumper impact level and defined as a frangible joint. The frangible joint is used to simulate leg fracture resulting

from duration of a lateral impact load. A detailed description of the breakable leg model was given in studies by Yang *et al.* (1993) and Yang (1997).

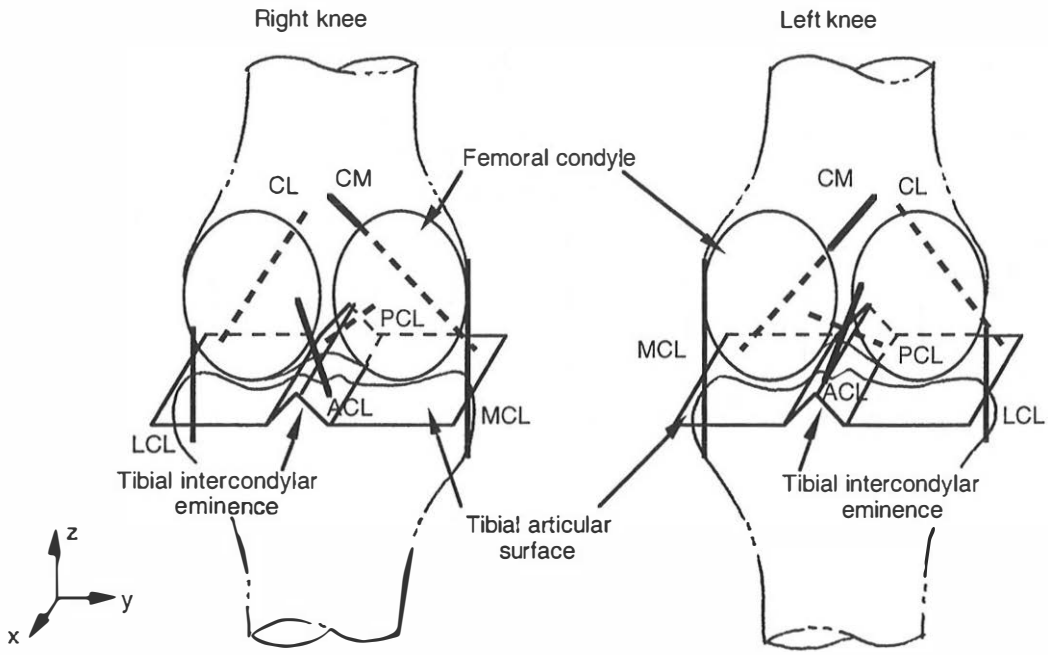

Figure 3. The mathematical model of the knee joints, ACL = anterior cruciate ligament; PCL = posterior cruciate ligament; MCL = medial collateral ligament; LCL = lateral collateral ligament; CM/CL = posterior part of the capsule. For simplification the attachment of the LCL is placed on the tibia.

COMPUTER SIMULATIONS OF THE CAR-PEDESTRIAN IMPACTS - Figure 4 shows the configuration for computer simulations of car-pedestrian impact tests with unembalmed cadaver specimens which represented a pedestrian impacted from the lateral side by a car-front. The human-body mathematical model was used to simulate the impact tests as shown in Table 5.

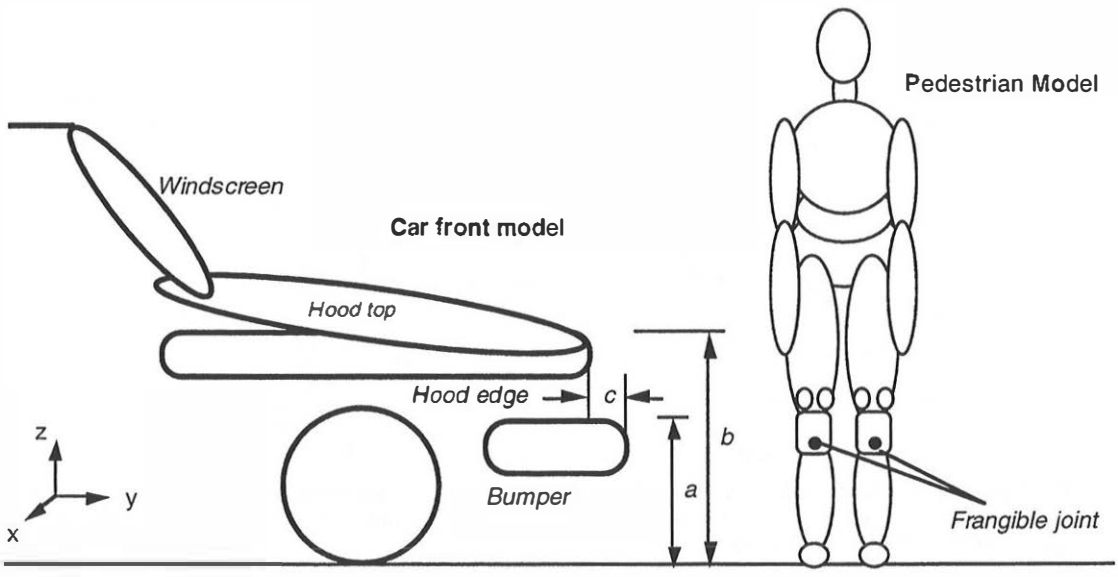

Figure 4. The set-up for computer simulation of the car-pedestrian impact tests, *a* = bumper height, *b* = hood edge height, *c* = bumper lead distance. The car-front model was based on Ishikawa *et al.* (1993).

Pedestrian mathematical models - In the simulations of the tests, each pedestrian substitute was simulated individually based on height and weight of the unembalmed cadaver subject which was registered with sex, age, height and weight in each test (Table 5). The position and posture of the

pedestrian mathematical models were adjusted according to the configuration of the cadaver specimens in the tests.

Car-front model - The car-front model consists of four ellipsoids and two hyperellipsoids. The bumper and hood-edge were represented by one hyperellipsoid for each, and the hood-top and windscreen were represented by one ellipsoid for each. The wheels were represented by two ellipsoids. The geometry and dimensions of the car-front model are shown in Figure 4 which was based on a experimental set-up (Ishikawa *et al.*, 1993). The bumper level *a* and hood-edge level *b* were adjusted based on the active levels of the bumper and the hood edge determined in the tests (Table 5). The location of center of gravity and moments of inertia for the car-front model was defined approximately, since the one-dimensional nature of the car motion in the tests. The stiffness characteristics of car fronts is shown in Figure 5.

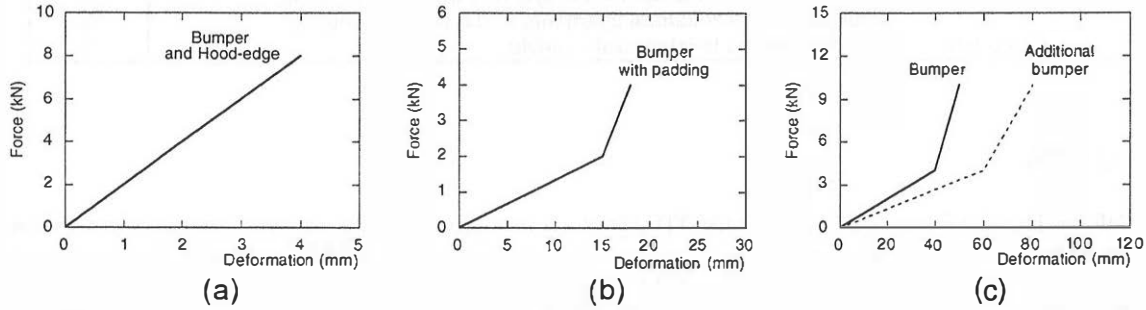

Figure 5. The stiffness characteristics of car fronts: (a) bumper in tests 1, 2 and 5, hood-edge for all tests; (b) in test 3; (c) in test 4 (based on Ishikawa *et al.*, 1993).

Contact characteristics were defined in the simulations for all possible impacts between body segments of pedestrian model and car-front components. The friction coefficient is 0.7 between foot and ground, 0.3 between body segments and car-front components.

VALIDATION OF THE HUMAN-BODY MATHEMATICAL MODEL

IMPACT TESTS WITH PEDESTRIAN SUBSTITUTES - The validity of the human-body mathematical model was evaluated by using published results from impact tests with cadavers (Ishikawa *et al.*, 1993). The available test configurations are shown in Table 5.

Table 5
The test matrix (based on Ishikawa *et al.*, 1993)

Test No.	Impact speed (km/h)	Bumper level* (mm)	Bumper-lead distance (mm)	Hood edge level* (mm)	Age/Sex of subject	Height of subject (mm)	Weight of subject (kg)
1	25	380	60	730	54/male	1800	75
2	32	380	60	730	48/male	1700	62
3	32	380	85	730	52/male	1780	65
4	32	440	100	730	53/male	1800	89
5	39	390	200	720	68/male	1750	88

* Effective level determined in tests.

In the tests, unembalmed cadavers were used as pedestrian substitutes which were struck by an car-front mounted on a sled from lateral side of the pedestrian substitute. Each cadaver specimen was positioned with a walking posture and the knee extended, balanced in an upright position. High-speed cameras were used to register trajectories of the pedestrian substitutes during impact tests. Impact responses of the pedestrian substitutes were measured with four accelerometers. The accelerometers were located in the following body segments:

- Head (3-axis accelerometer close to the center of gravity of the head),
- Thorax (3-axis accelerometer mounted at the thoracic vertebra T6),
- Pelvis (3-axis accelerometer mounted at the lumbar vertebra L5),
- Leg (1-axis accelerometer at the tibia 15 - 20 cm from the sole of the foot).

Damage of each cadaver specimen were identified by means of anatomical investigations after impact tests. The main findings of body segment damage are summarized in Table 6.

Table 6
Damage to pedestrian substitutes in impact tests (based on Ishikawa *et al.* 1993)

Test No.	Body segments	Damage description	AIS
1		No visible damage.	-
2	Leg	Fibula fracture and tibia fracture of the first impact leg.	3
3	Leg	Fibula fracture and tibia fracture of the first impact leg.	3
	Neck	Fracture of cervical vertebra C7.	3
4	Head	Abrasion of the face skin.	2
5	Scull	Fracture of scull right side.	5
	Knee right	Fracture of the tibial lateral condyle and the head of fibula;	3
		Rupture of the collateral ligaments and crucial ligaments.	3
	Knee left	Fracture of the tibial medial condyle.	3

RESULTS

KINEMATICS OF PEDESTRIAN SUBSTITUTES - A comparison between the simulations and the tests for the kinematics of the pedestrian substitutes is shown in Figure 6. The overall kinematics of the pedestrian models from computer simulations appear to be well in agreement with observations from the high-speed films in impact tests. For detail body segment motion, a good agreement between the simulations and the tests for leg rotation around knee joint in the initial phase of impacts can also be seen from Figure 6. The occurrence and location of the head-hood impact was realistically predicted by the pedestrian models. The head-hood impact occurred from about 150 ms to 200 ms and occurred earlier at high impact speed than low speed.

PEAK VALUES AND TIME HISTORIES OF THE INJURY RELATED PARAMETERS - The output data from computer simulations of car-pedestrian impact are shown in Table 7. The time histories of the linear accelerations for the leg, the pelvis, and the head from the test 4 and corresponding computer simulation are shown in Figures 7. The time histories of the linear accelerations for the thorax, the pelvis, and the head from the test 5 and corresponding computer simulation are shown in Figures 8.

Impact forces - The peak bumper impact forces to the leg changed with different impact speeds. The impact forces varied from 4.4 kN to 9.3 kN in the computer simulations (Table 7). The peak impact forces increase with the increasing impact speed in the simulations, except for impact force from test 4 in which a double-bumper with lower stiffness than other bumpers was used.

Table 7
Peak values from computer simulations

Run No.	1 (V=25km/h)	2 (V=32km/h)	3 (V=32km/h)	4 (V=32km/h)	5 (V=39km/h)
Impact force (kN)	4.4	7.6	6.3	4	9.3
Leg Acc. (g)	131	198	188	138	228
Thigh Acc. (g)	124	125	98	87	156
Pelvis Acc. (g)	33	65	29	38	82
Chest Acc. (g)	18	21	28	25	32
Head Acc. (g)	86	125	157	117	248

Accelerations - The peak accelerations of the leg varied from 131g to 228 g in the simulations, and the measured leg accelerations available in the test 4 is 135 g (Figure 7a) at an impact speed of 32 km/h. The peak accelerations of the thighs varied from 87g to 156 g in the simulations. The chest accelerations varied from 18 g to 32 g in the simulations, and the measured chest acceleration available in test 5 is 48 g (Figure 8a). The pelvis accelerations varied from 33 g to 82 g in the simulations, and 52 g to 78 g in the tests (Figure 7b and Figure 8b). The head resultant accelerations varied from 86 g to 248 g in the simulations. The measured head resultant accelerations available in the test 4 and 5 is 125 g and 280 g (Figure 7c and Figure 8c), respectively.

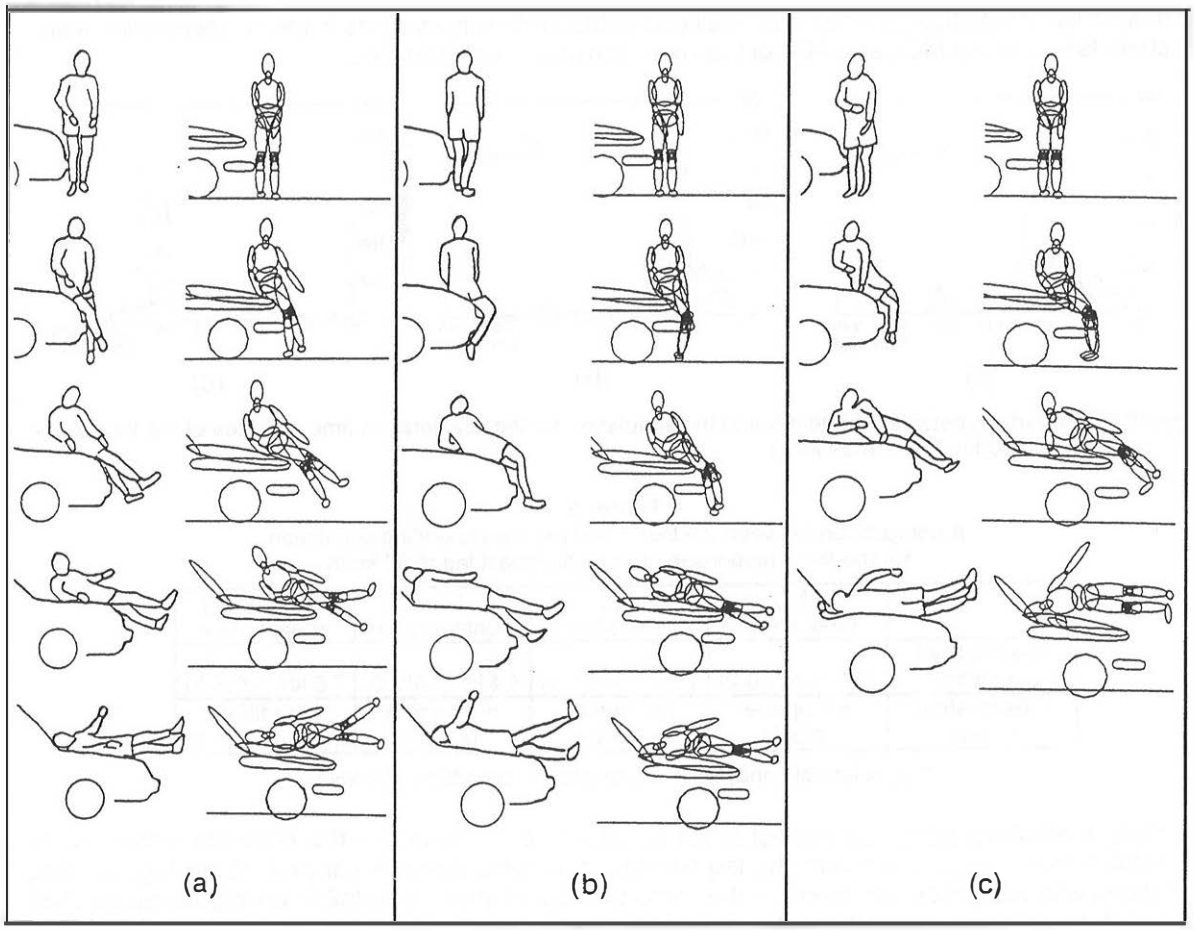

Figure 6. Comparison between the tests (1, 3, 5) (Ishikawa *et al.*, 1993) and corresponding simulations for kinematics of the pedestrian substitutes at impact speeds of (a) 25 km/h, (b) 32 km/h, and (c) 39 km/h, time step $\Delta t = 50$ ms.

Figure 7 shows the accelerations of the leg and head measured in the test 4 are well predicted in the simulation with the pedestrian model in terms of the peak values and the curve wave shapes. The peak values of the pelvis acceleration were underestimated in the simulation. Figures 8 shows the accelerations of the pelvis from the cadaver specimen test 5 and the simulation were very similar regarding the peak values and curve wave shapes. The peak values of the thorax acceleration were underestimated in the simulation.

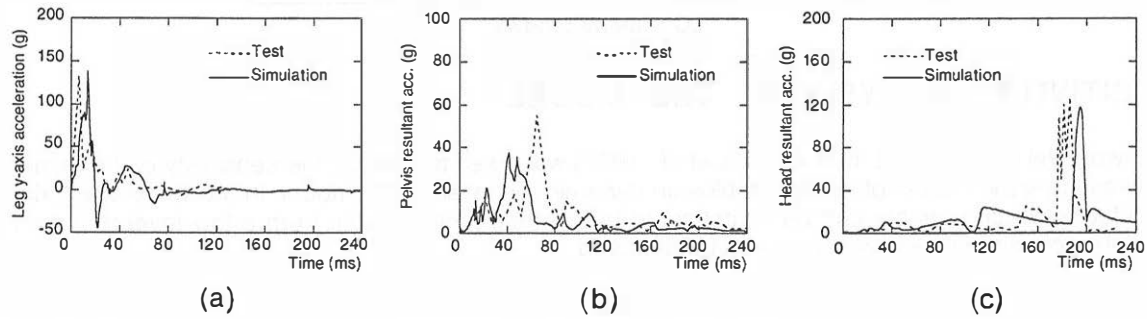

Figure 7. Comparison between the test 4 and the simulation for the acceleration time histories of the leg, the pelvis, and the head at 32 km/h.

Responses of the knee - Knee responses in the simulations were predicted in terms of ligament strain, and contact force between articular surfaces. A comparison between the test 2 and corresponding simulation at a speed of 32 km/h was made for the knee responses to car frontal impact. Table 8 shows the comparison for responses of MCL and ACL of the first impact leg, and the lateral condyle contact force between articular surfaces of the knee. Based on the study on strength of knee ligaments (Butler *et al.*, 1986), ligament rupture failure is defined at strain greater than 20%. The

calculated ligament strains for the knee well correlated to the observations in the corresponding test in which no failure to the MCL and ACL of the knee were observed (Table 8).

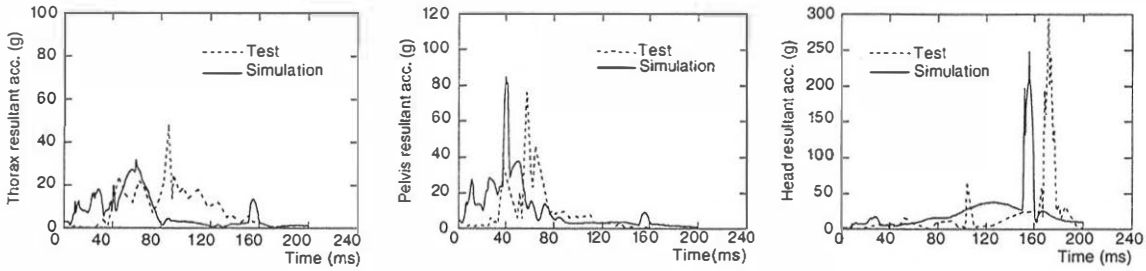

(a) (b) (c)

Figure 8. Comparison between the test 5 and the simulation for the acceleration time histories of the thorax, the pelvis, and the head at 39 km/h.

Table 8
A comparison between the test 2 and the corresponding simulation for the knee responses of the first impact leg at 32 km/h

	MCL peak strain	ACL peak strain	LC* contact force	Bumper-leg impact force
Results from simulation	17% (~AIS 0-2)	14% (~AIS 0-1)	4.4 kN (~AIS 0)	7.6 kN (~AIS 3)
Observation in test	no rupture (AIS 0)	no rupture (AIS 0)	no fracture (AIS 0)	tibia/fibula fracture (AIS 3)

* LC = lateral condyle. (~) correlated to possible injury level.

Knee responses with and without leg fracture - In order to detect the knee responses in the pedestrian model associated with the leg fracture, two simulations of car-pedestrian impacts was performed with the pedestrian model in the same configuration of the tests2 at an impact speed of 32 km/h. Table 9 shows the results of the knee responses with and without leg fracture for the strains of MCL and ACL of the first impact knee, and the lateral condyle contact forces. The calculated MCL and ACL strains as well LC contact force in case of no leg fracture were higher than that in case of leg fracture.

Table 9
Responses of the knee with and without leg fracture in simulations for the same configuration of test 2 at 32 km/h

	MCL peak strain	ACL peak strain	LC* contact force
Leg fracture	17%	14%	4.4kN
No leg fracture	57%	60%	12.5kN

* LC = lateral condyle.

SENSITIVITY ANALYSIS OF THE MODEL

A two-level factorial test method (Box *et al.*, 1978) was used to analyze the sensitivity of the model and investigate the effects of input variables on dynamic response of the model. In a two-level factorial test, effect of each variable can be investigated by changing the variable from a low level to a high level. Interactions between variables can be detected.

Table 10
The factors and levels for sensitive study

Factors	Levels	
	–	+
A=Bumper height	275 mm	500 mm
B=Bumper stiffness	100 N/mm	300 N/mm
C=Bumper lead distance	50mm	200 mm
D=Hood-edge height	600 mm	800 mm
E=Hood-edge stiffness	1000 N/mm	2000 N/mm
F=Impact speed	15 km/h	40 km/h

FACTORIAL TEST - The parameters used in the present study are: bumper height, bumper stiffness, bumper lead distance, height of hood-edge, hood-edge stiffness, and impact speed. The selected variables and levels are shown in Table 10. The bumper levels were chosen between knee joint and center of gravity of the leg for a 50th percentile male adult, and the hood-edge levels between hip joint and knee joint. A reduced factorial test design of 32 runs was made based on the selected factors and levels.

RESULTS OF FACTORIAL TEST - Selected output parameters from computer simulations are impact force, knee rotation angle, MCL ligament strain, head angular acceleration, and HIC.

The sensitivity of the pedestrian mathematical model to the change of the car-front parameters and impact speed was studied by means of the responses of the model in the simulations. Figure 9 shows the calculated effects of one-factor and two-factor on the injury-related output parameters based on results from 32 simulation runs. Mean responses for two-factor interactions were calculated with the output parameters. Part of the calculated mean responses is shown in Figure 10 in the form of mean response diagram. Absence/presence of interaction between two factors can be detected in the diagrams, and effects of each factor in two selected levels on the responses of the model can also be analyzed by means of these diagrams.

Effect of impact speed on responses of the model - A significant effect of impact speed on the responses of the model for almost all parameters can be seen from Figure 9. Only head angular acceleration appears to be dependent primarily on hood-edge height.

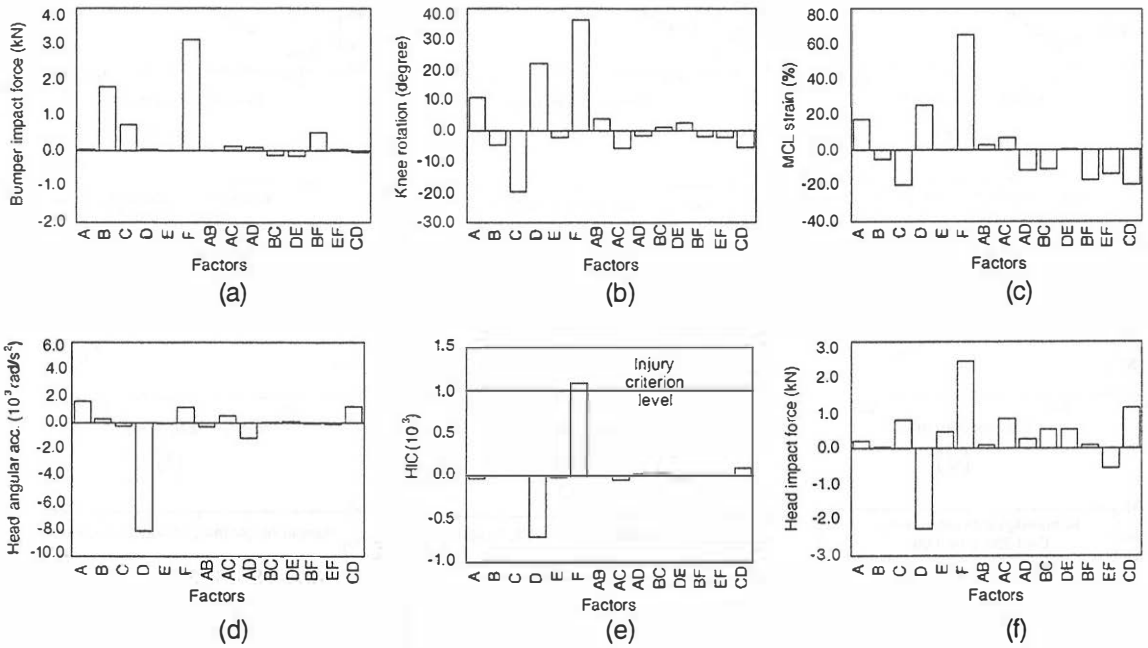

Figure 9. Effects of one-factor and two-factor on output parameters: (a) Bumper impact force, (b) knee rotation angle, (c) MCL strain, (d) head angular acceleration, (e) HIC, and (f) head impact force.

Effect of bumper and hood-edge on responses of lower extremity - Figure 9a, b, and c show significant effects of the bumper height, bumper stiffness, bumper lead distance, and hood-edge height on responses of the knee-leg complex in a lateral impact to the leg.

From Figure 10a, it can be seen that the bumper impact forces are sensitive to the change of the bumper stiffness. The impact force to the leg goes up by 48% when the bumper stiffness increases from 100 N/mm to 300 N/mm. There is almost no effect of bumper height on the impact force. There is less effect of bumper stiffness on knee responses especially at high bumper level (Figure 11b and c).

There is a significant effect of bumper height to the knee rotation angle and MCL strain. Figure 10b shows the knee rotation angle increases 69% when the bumper height changes from 275 to 500 mm for the bumper stiffness 300 N/mm. The MCL strain increases 53% with the increasing bumper height from 275 to 500 mm for the bumper stiffness 300 N/mm (Figure 10c).

Bumper lead distance have significant effect to the MCL strain and the knee rotation angle. Figure 10d shows that the MCL strain decreases 47% for the bumper lead from 50 mm to 200 mm at the low bumper height. The MCL strain decreases 17% with the increasing bumper lead distance from 50 mm to 200 mm at the high bumper level. When the bumper lead distance increases from 50 mm to 200 mm the knee rotation angle decreases by 52% at a bumper height of 500 mm (Figure 10e). Figure 10f shows an interaction between bumper lead and hood-edge stiffness. A significant effect of bumper lead on the MCL strain can be seen in combination with a hood-edge stiffness of 2000 N/mm.

Figure 10g shows that the knee rotation angle reduced by 49% when the hood-edge height decreases from 800 to 600 mm in the case of hood-edge stiffness 2000 N/mm. The stiffness of the hood-edge have less effect on knee rotation.

The knee responses in the simulations of car-pedestrian impacts are sensitive to the changes of the bumper and hood-edge parameters, especially for the varied bumper and hood-edge height as well as bumper lead distance. The knee responses are dependent primarily on the shape of the car-front end.

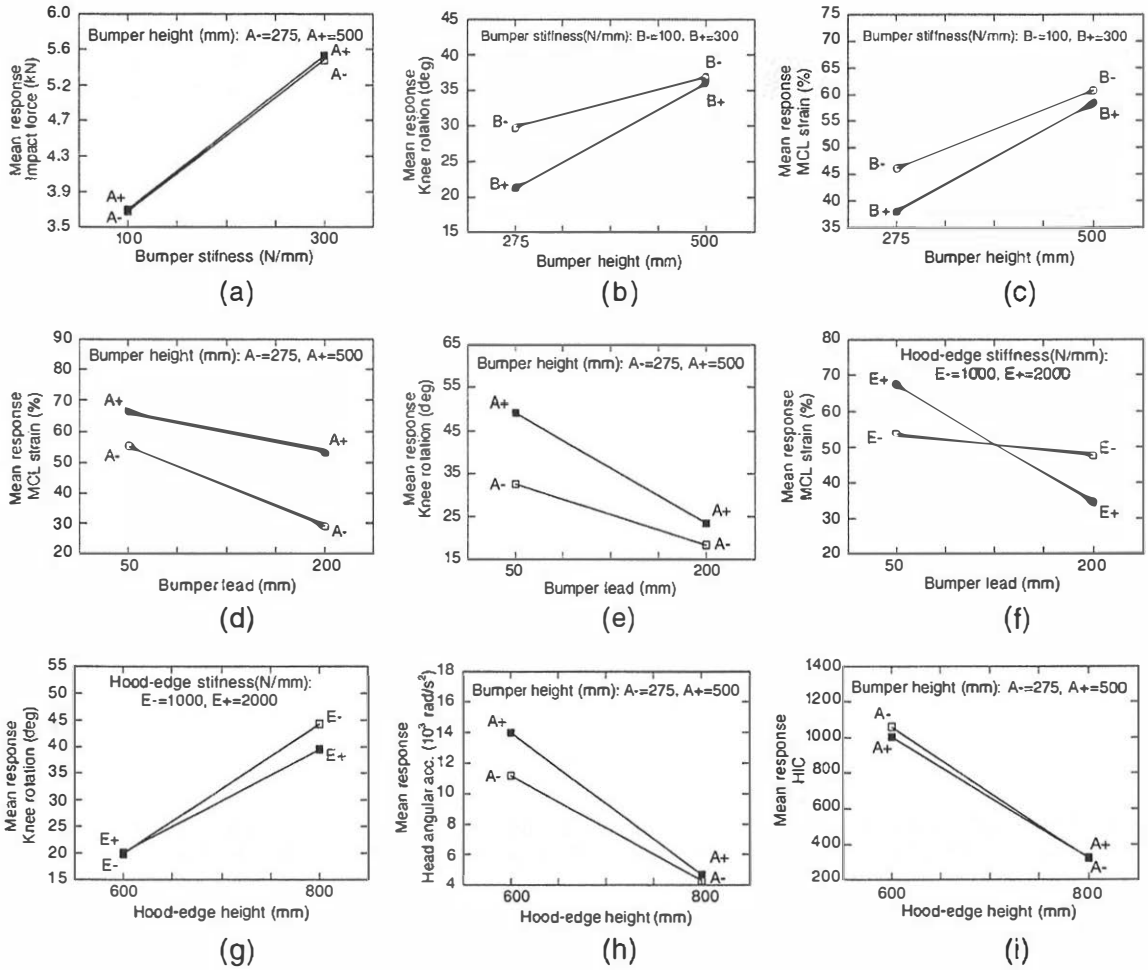

Figure 10. Mean response diagrams between two factors: (a) bumper stiffness and height, (b, c) bumper height and bumper stiffness, (d, e) bumper lead and bumper height, (f) bumper lead and hood-edge stiffness, (g) hood-edge height and hood-edge stiffness, and (h, i) hood-edge height and bumper height.

Effect of bumper and hood-edge on head responses - Figure 10h and i show two-factor interactions between hood-edge height and bumper height in terms of the head angular acceleration and the HIC value. Hood-edge height has a significant effect to the head response. With an increasing hood-edge height from 600 mm to 800 mm, the head angular acceleration decreases by 61% for low bumper level and by 66% for high bumper level, while the HIC value decreases by 70%. There is almost no effect of bumper height on the HIC values.

DISCUSSION

Twenty years ago, Padgaonkar *et al.* (1977) pointed out that experimental studies of the effects of all the variables in car-pedestrian impacts are impractical, and this is still the case today due to the lack of available pedestrian substitutes and difficulties in measurements in laboratory crash tests. An alternative approach is the use of a well-validated pedestrian mathematical model to study this type of impact. Accordingly, the present study attempted to develop a pedestrian mathematical model which can be used in simulations of car-pedestrian impacts. Since pedestrian fatalities in accidents have mainly been attributed to head injuries, and the lower extremity injuries occurred often with long term consequence. Thus, the main focus was on modeling responses of lower extremities and head in a lateral car-front impact.

The kinematics in car-pedestrian impacts are quite complex due to successive impacts to the body segments in a large relative movement between pedestrian and moving car. A good correlation of the kinematics between the simulated and measured results gives certain level of confidence to verify the calculated parameters from the model.

The overall kinematics of pedestrian substitutes in impact tests were realistically simulated with the pedestrian mathematical model (Figure 6). Good flexibility was obtained in the model. The lateral rotation of the pedestrian substitutes in the impact tests, especially the head rotation around the neck joint as well as the knee rotation around the bumper, were well predicted in the simulations. The occurrence and the location of the head impact to the hood (Figure 6) indicated that the head impact area on the hood were correctly simulated. These could be attributed to the better formulation of the pedestrian mathematical model than that of dummy-based pedestrian model in terms of the following key points. First, the joint characteristics were defined based on studies (Table 3 and 4) of the joint physiology movement and joint biomechanics, which makes the model flexible and comparable with human joint flexibility. Second, the knee joint model was formulated based on an anatomical knee structure, therefore the responses of the knee model are well correlated with the knee responses in the tests. Third, the breakable-leg model fills the gap of modeling leg fracture. Finally, the force-deflection characteristics were defined to take into account the mutual deformability of the body segments and the car-front surfaces. The definition of mechanical properties in the model were based on studies of strength and tolerance of the human body segments. There are no universal constants to characterize the properties of human tissues or to predict its response to a given boundary condition. In the crash environment of car-pedestrian accidents, the pedestrians are frequently struck from the lateral side, therefore the data from studies (Stalnaker *et al.*, 1977; Cesari *et al.*, 1981; Nyquist *et al.*, 1985; Viano, 1989; Allsop *et al.*, 1991) on human tolerance in a lateral impact condition were chosen to best suit the configuration of car-pedestrian impacts. The selected data from these studies provided a framework to appropriately characterize the model.

The tests and simulations for body segment responses were compared in terms of accelerations, indicating that the accelerations in the simulations approximate the results from the tests. The accelerations of the head, the pelvis, and the leg, calculated in simulations, appear to be in good agreement with the available results measured in tests in both peak value and curve shape. Although the accelerations of the head and the leg in the tests were not all available, the calculated results show a reasonable trend of increasing accelerations with the increasing impact speed. The acceleration of the pelvis in the simulation of test 4 at 32 km/h and the acceleration of the thorax in the simulation of test 5 at 39 km/h were underestimated compared with the test results (Figures 7b and 8a). This difference could be attributed to contact between forearm and hood. The initial position of forearm-hood impact may vary due to the fact that the forearm movement during the simulations was free. Another explanation is that the forearm in combination with the hand may introduce excessive stiffness due to the absence of the wrist joint. The occurrence of the peak values of the accelerations (Figure 8) may also influenced by the forearm-hood contact.

Furthermore, some calculated parameters, which could not be measured in the tests, are comparable with findings from anatomical investigations after impact tests. For instance, the ligament ruptures were attributed to ligament strain when it exceeds the tolerance level. The knee ligament strains calculated in the present model can be used to predict the risk of ligament ruptures. The calculated bumper impact force in the knee joint area and contact forces between articular surfaces can be used to predict the risk of condyle fractures.

The results from the factorial test clearly show the effects of the input variables on responses of the model. The coupling between variables is generally low (Figure 9 and 10). The sensitivity of the model to the input variables can be detected based on the factorial test. The model is sensitive to impact speed for almost all injury-related parameters. The lower extremity in the model is sensitive to the changes of bumper stiffness, bumper height, bumper lead distance, hood-edge height. The head

in the model is sensitive to the variation of the hood-edge height, especially in predictions of head angular-acceleration. It was confirmed that the head response is significantly influenced by hood-edge height of car. The breakable leg model improved the sensitivity of the knee responses associated with leg fracture in certain impact condition.

Unlike engineering materials, material properties of human tissues are dependent on many non-engineering factors of the human. However, the mechanical properties of body segments were defined with average values based on published data, and variations in the data due to age, gender and population differences were not taken into account in the current model. It could be one of the causes to introduce the deviation between the simulations and cadaver tests. For this reason, it can be expected that the simulation results can better fit a test corridor than a single test curve available at the present study.

It is necessary to point out that the pedestrian mathematical model was validated by using tests with cadaver specimens, therefore the deviation between simulations and real world accidents should also be noted. For instance, soft tissues was simulated with a simple model, so that soft tissue effect may not be adequately represented.

The current breakable leg model only simulates a single leg fracture, consequently it is hard to connect the simulation results to a more complicated long bone multiple fractures. For simulations of such fractures, it is necessary to refine the model or to develop a FEM model that can predict the bone failures by calculating stress concentration within the bone structure and modeling multiple fractures.

Despite the limitations in the current model due to the complexity of the impact event, the results from the present study indicate its capability of calculating relevant parameters to predict risk of injuries to pedestrian body segments. For instance, the impact forces or bending moments on the thighs and legs can be calculated to predict risk of long bone fractures. For the knee, the forces and moments transferred through the knee components, as well as the strain of the knee ligaments can be calculated to evaluate the knee failures in lateral impact loading. For the head, the linear acceleration, the HIC value and the angular acceleration can be calculated to predict risk of head injuries. The model is thus useful for simulation of car-pedestrian impacts and for performance assessment of car-front structures.

In the near future, a subsystem test method proposed by EEVC (1994) will be issued as an international regulation to evaluate car fronts for pedestrian protection. The subsystem test method consists of three separate tests using a head-form impactor, a thigh-form impactor, and a leg-form impactor. The subsystem tests can measure the performance of car-front components separately, but interactions of car-front parameters to responses of different body segments can not be detected by such tests. As already mentioned, the pedestrian mathematical model used in simulations of car-pedestrian impacts provides not only the information about the head responses to the hood or windscreen impact but also the information about the influence of changes of car-front-end shape on head responses. Therefore, the model, as an important complement to subsystem tests, is valuable for investigating possible improvements of new car-front designs by providing insight into pedestrian impact protection.

For further study on pedestrian impact protection using the developed human-body mathematical model, the head-neck and thorax segments should be improved to simulate detailed responses in these body regions. The model should allow for the investigation of the risk of brain and neck injuries and the study of thorax injuries in terms of TTI (thoracic trauma index) and VC (viscous criterion). Sophisticated biomaterial models are also needed if better correlation with pedestrian responses in real world accidents is to be achieved.

CONCLUSIONS

Research into the vehicle-pedestrian accidents during the past three decades has indicated that there is a need for a biofidelic model of the human body in order to study injury biomechanics of pedestrians in vehicle impacts and to acquire better understanding of this type of impacts for developing safety countermeasures.

The developed human-body mathematical model is able to simulate the responses of pedestrians in car impacts. A good kinematic correlation between the model and the test subjects was achieved for both overall movement and body segment motion.

The important injury-related parameters can be calculated by means of the model, including impact forces, accelerations for different body segments, HIC, contact forces between articular surfaces, and knee ligament strain. It is therefore valuable for the prediction of risk of pedestrian injuries in accidents.

The model is sensitive to the change in car-front parameters and impact speeds, and is thus a useful tool for analyzing pedestrian responses in different impact conditions and studying the performance of the vehicle exterior for pedestrian protection.

ACKNOWLEDGEMENT

We would like to thank ECIA - Equipements et Composants pour L'industrie Automobile, France, for sponsoring this study.

REFERENCES

Aldman, B., Kajzer, J., Bunketorp, O. and Eppinger, R. (1985): An Experimental Study of a Modified Compliant Bumper. 10th International Technical Conference on Experimental Safety Vehicles, Oxford, England.

Allinger, T.L. and Engsberg, J.R. (1993): A Method to Determine the Range of Motion of the Ankle Joint Complex, In Vivo. J. Biomech. 26(1):69-76.

Allsop, D.L., Perl, D.R. and Warner, C.Y. (1991): Force/Deflection and Fracture Characteristics of the Tomporo-Parietal Region of the Human Head. Proc of *the 35th Stapp Car Crash Conference*, SAE, Warrendale, PA, USA.

Appel, H., Kühnel, A., Stürtz, G. and Glöckner, H. (1978): Pedestrian Safety Vehicle - Design Elements- Results of In-Depth Accident Analyses and Simulation. 22nd AAAM Conf. and the Int. Association for Accident and Traffic Medicine, Ann Arbor Michigan, USA.

Ashton, S.J. (1978): Cause, Nature, and Severity of the Injuries Sustained by Pedestrians struck by the Fronts of Cars or Light Goods Vehicles. University of Birmingham.

Baughman, L.D. (1983). Development of an Interactive Computer Program to Produce Body Description Data. AFAMRL-TR-83-058, Air Force Aerospace Medical Research Laboratory, Wright-Patterson Air Force Base, Ohio, USA.

Begeman, P.C. and Prasad, P. (1990): Human Ankle Impact Response in Dorsiflexion. Proc. of the 34th Stapp Car Crash Conference, SAE, Warrendale, PA, USA, pp. 39-54.

Bowman, B. M., Schneider, L. W., Lustak, L. S. and Anderson, W. R. (1984). Simulation Analysis of Head and Neck Dynamic Response. Proc. of the 28th Stapp Car Crash Conference, Society of Automotive Engineers, Warrendale, PA, USA. p. 173.

Box, G.E.P., Hunter, W.G. and Hunter, J.S. (1978). Statistics for Experimenters, An Introduction to Design, Data Analysis and Model Building. John Wiley & Sons, New York.

Brun-Cassan, F., Tarriére, C., Fayon, A. and Mauron, G. (1983). Comparison of Behaviours for PART 572 and APROD Dummies Tested as Pedestrians Impacted by a Car, Under Identical Test Conditioning. Proc. of the Pedestrian Impact Injury & Assessment. SAE Int. Congress & Exposition, P-121, Detroit Michigan, February 28-March 4. Warrendale, USA. pp. 129-137.

Bunketorp, O., Aldman, B., Eppinger, R., Romanus, B., Thorngren, L., Hansson, T (1983): Experimental Study of a Compliant Bumper System', the joint IRCOBI-STAPP Conference, San Diego, USA.

Butler, D.A, Kay, M.D. and Stouffer, D.C. (1986): Comparison of Material Properties in Fascicle-Bone Units from Human Patellar Tendon and Knee Ligaments. *J. Biomechanics*, 1986, **19**, 425-432.

Cavallero, C., Cesari, D., Ramet, M., Billault, P., Farisse, J., Seriat-Gautier, B. and Bonnoit, J (1983): Improvement of Pedestrian Safety: Influence of Shape of Passenger Car-Front Structures Upon Pedestrian Kinematics and Injuries: Evaluation Based on 50 Cadaver Tests. Proc. of the Pedestrian Impact Injury & Assessment. SAE Int. Congress & Exposition, P-121, Detroit Michigan, SAE, Warrendale, PA, USA.

Cesari, D. and Ramet, M. (1982). Pelvic Tolerance and Protection Criteria in Side Impact. Proc. 26th STAPP Car Crash Conference, Ann Arbor USA. pp. 145-154.

Cesari, D., Ramet, M. and Bloch, J. (1981). Influence of Arm Position on Thoracic Injuries in Side Impact. Proc. of the 25th Stapp Car Crash Conference, Society of Automotive Engineers, Warrendale, PA, USA. pp. 271-297.

Cesari, D., Ramet, M. and Zac, R. (1982). Behaviour of Side Impact Dummies Used as Pedestrians in Accident Reconstructions. Proc. of the 7th Int IRCOBI Conf on the Biomechanics of Impacts, Köln, Sept 8-10. IRCOBI Secretariate Bron France. pp. 230-240.

EEVC (1985). Pedestrian Injury Protection by Car Design. Proc. of the Tenth Int. Tech. Conf. on Experimental Safety Vehicles, Oxford England, July 1-4, 1985. US Dept. of Transportation, NHTSA, USA. pp. 965-976.

EEVC (1994): Proposals for Methods to Evaluate Pedestrian Protection for Passenger Cars. Report, *European Experimental Vehicle Committee*, working group 10.

ETSC (1993). Reducing Traffic Injuries through Vehicle Safety Improvements - The Role of Car Design. European Transport Safety Council, Brussels.

ETSC (1997). A StrategicRoad Safety Plan for the European Union. European Transport Safety Council, Brussels.

Frankel VH, Nordin M. Basic Biomechanics of the Skeletal System.Philadelphia, USA: Lea & Febiger, 1980

Gibson, T. J., Hinrichs, R W., McLean, A J. (1986). Pedestrian Head Impacts: Development and Validation of a Mathematical Model. Proc. of the Int IRCOBI Conference on Biomechanics of Impacts. September 2-4, Zürich. IRCOBI Secretariat, Bron France. pp 165-176.

Glaeser, K. P. (1983). Step to Step Approach to a Standardized Full Scale Pedestrian Test Methodology. Proc. of the Pedestrian Impact Injury & Assessment. SAE Int. Congress & Exposition, P-121, Detroit Michigan, February 28 - March 4. Warrendale, USA. pp. 93-101.

Ishikawa, H., Kajzer, J. and Schroeder, G. (1993). Computer Simulation of Impact Response of the Human Body in Car-Pedestrian Accidents. Proc. of the 37th Stapp Car Crash Conference, November 8-10, San Antonio, Texas. SAE, Warrendale, PA, USA. pp. 235-248.

Janssen, E. G. and Wismans, J. (1986). Experimental and Mathematical Simulation of Pedestrian-Vehicle and Cyclist-Vehicle Accidents. Proc. of the 10th Int. Technical Conf. on Experimental Safety Vehicle, Oxford England, July 1-4, 1985. US Dept of Transportation, NHTSA. pp. 977-988.

Kapandji, I. A. (1970a). The Physiology of the Joints. Volume One. Upper Limb. Press of the Churchill Livingstone.

Kapandji, I. A. (1970b). The Physiology of the Joints. Volume Two. Lower Limb. Press of the Churchill Livingstone.

Kapandji, I. A. (1970c). The Physiology of the Joints. Volume Three. The Trunk and the Vertebral Column. Press of the Churchill Livingstone.

Kramer, M., Burow, K. and Heger, A. (1973): Fracture Mechanisms of Lower Legs Under Impact Load. 17th Stapp Car Crash Conference, Oklahoma City, USA.

Kress, T. A., Snider, J. N., Porta, D. J., Fuller, P. M., Wasserman, J. F. and Tucker, G. V. (1993). Human Femur Response to Impact Loading. Proc. of the Int. IRCOBI Conf. on the Biomechanics of Trauma, September 8-10, Eindhoven, the Netherlands. IRCOBI Secretariat, Bron, France. pp. 93-104.

McElhaney, J. H., Doherty, B. J., Paver, J. G., Myers, B. S. and Gray, L. (1988). Combined Bending and Axial Loading Responses of the Human Cervical Spine. Proc. of the 32nd Stapp Car Crash Conference, Society of Automotive Engineers, Warrendale, PA, USA. pp. 21-28.

Mertz, H. J. and Patrick, L. M. (1971). Strength and Response of the Human Neck. Proc. of the 15th Stapp Car Crash Conference, Society of Automotive Engineers, Warrendale, PA, USA.

Messerer, O. (1880). Uber Elasticitat und Festigcitat der Mnschlichen Knochen. Stuttgard.

Mohan, D., Kajzer, J., Bawa-Bhalla K.S., Chawla, A., Sarabjit, S. (1995). Impact Modeling Studies for a Three-Wheeled Scooter Taxi. Proc. of the 1995 International IRCOBI Conference on the Biomechanics of Impacts, Sept 13-15, Brunnen, Switzerland, pp 325-336, .

Nahum AM, and Melvin J. (1985): The Biomechanics of Trauma.Norwalk, CT, USA: A.C.C, Prentice-Hall, Inc.

NHTSA (1995). Traffic Safety Facts 1994. National Highway Traffic Safety Administration, US Dept of Transportation, Washington DC, USA.

Niederer, P. F., Schlumpf, M., Mesqui, F. and Hartmann, P.-A. (1983). The Reliability of Anthropometric Test Devices, Cadavers, and Mathematical Models as Pedestrian Surrogates. Proc. of the Pedestrian Impact Injury & Assessment. SAE Int. Congress & Exposition, P-121, Detroit Michigan, February 28-March 4. Society of Automotive Engineers, Warrendale, USA. pp. 119-128.

Nyquist, G W, Cheng, R., El-Bohy, AAR and King, A I (1985) Tibia Bending: Strength and Response. 29th Stapp Car Crash Conference, Warrendale, PA, USA.

Nyquist, G. W. and Murton, C. J. (1975). Static Bending Response of the Human Lower Torso. Proc. of the 19th Stapp Car Crash Conference, Society of Automotive Engineers, Warrendale, PA, USA.

Padgaonkar, A. J., Krieger, K. W. and King, A. I. (1977). A Three-Dimensional Mathematical Simulation of Pedestrian-Vehicle Impact With Experimental Verification. Transactions of the ASME, *Journal of Biomechanical Engineering*, May 1977, pp. 116-123.

Panjabi, M. M., Summers, D. J., Pelker, R. R., Vidoman, T., Friendlander, G. E. and Southwick, W. O. (1986). Cervical Spine Biomechanics. J. Orthop. Res., (:4). pp. 152 - 161.

Parenteau, C. S., Viano, D. C. and Petit, P. Y. (1996). Biomechanical Properties of Ankle-subtalar Joints in Quasi-Static Loading to Failure. *J. Biomechanical Engineering*. (Submitted).

Pritz, H.B. (1978): Comparison of the Dynamic Responses of Anthropomorphic Test Devices and Human Anatomic Specimens in Experimental Pedestrian Impacts', 22nd Stapp Car Crash Conference, Ann Arbor Michigan, USA.

Schlumpf, M. R. and Niederer, P. F. (1987). Motion Patterns of Pedestrian Surrogates in Simulated Vehicle -Pedestrian Collisions. *J. Biomechanics,* **20**(:4). pp. 371-384.

Stalnaker, R. L., Melvin, J. W., Nusholtz, G. S., Alem, N. M. and Benson, J. B. (1977). Head Impact Response. Proc. of the 21st Stapp Car Crash Conference, Paper 770921, Society of Automotive Engineers, Warrendale, PA, USA.

TNO (1996): MADYMO User's Manual 3D. Version 5.2, Road-Vehicles Research Institute, Delft, The Netherlands.

van Wijk, J., Wismans, J., Maltha, J., Wittebrood, L. (1983). MADYMO Pedestrian Simulations. SAE paper 830060, P-121, . Pedestrian Impact & Assessment, Int. Congress and Exposition, Detroit, USA. pp. 109-117.

Viano, D. C. (1989). Biomechanical Responses and Injuries in Blunt Lateral Impact. Proc. of the 33rd Stapp Car Crash Conference, SAE, Warrendale, PA, USA. pp. 113-142.

Viano, D. C., Lau, I. V., Asbury, C., King, A. I. and Begeman, P. (1989). Biomechanics of the Human Chest, Abdomen, and Pelvis in Lateral Impact. Proc. of the 33rd Annual Conf. of Association for the Advancement of Automotive Medicine, AAAM, Des Plaines, IL. pp. 367-382.

Voigt, G. E., Hodgson, V. R. and Thomas, L. M. (1973). Breaking Strength of the Human Skull vs. Impact Surface Curvature. Report Contract No. DOT HS 146.2.230.

White, A. A. and Panjabi, M. M. (1978). Biomechanics of the Spine. Lippincott, Philadelphia.

Wismans, J. S. and Spenny, C. (1983). Performance Requirements of Mechanical Neck s in Lateral flexion. Proc. of the 27th Stapp Car Crash Conference, Society of Automotive Engineers, Warrendale, PA, USA. pp. 137.

Wismans, J., Van Dorschot, H. and Walttring, H. J. (1986). Omni-directional Human Head-Neck Response. Proc. of the 30th Stapp Car Crash Conference, Society of Automotive Engineers, Warrendale, PA, USA. pp. 313.

Wismans, J., van Wijk, J. (1982). Mathematical Models for the Assessment of Pedestrian Protection Provided by a Car Contour. Proc. of the 9th Int Techn Conf on ESV, Kyoto Japan Nov 1-4, US DOT NHTSA, pp 205-213.

Yamada, H. (1970). Strength of Biological Materials. Evans, F.G., Ed., Williams & Wilkens, Baltimore.

Yang, J.K. and Kajzer, J. (1993): Computer Simulation of Impact Response of the Human Knee Joint in Car-Pedestrian Accidents. SAE Transactions - *Journal of Passenger Cars*, V101-6, SAE Warrendale, PA, USA.

Yang, J. K., Rzymkowski, C. and Kajzer, J. (1993): Development and validation of a mathematical breakable leg model. Proc of the Int. IRCOBI Conf. on the Biomechanics of Trauma, Eindhoven, the Netherlands. IRCOBI Secretariat, Bron, France, pp. 175-186.

Yang, J.K., Kajzer, J., Cavallero, C., Bonnoit, J.(1995): Computer Simulation of Shearing and Bending Response of the Knee Joint to a Lateral Impact. Proc. of the 39th STAPP Car Crash Conference, Coronado, California, USA, pp. 251-264.

Yang, J.K. (1997): Mathematical Simulation of Knee Responses with Leg Fracture in Car-pedestrian Accidents. *International Journal of Crashworthiness*, Vol. **2** (:3), 1997.